Itinerant magnetism in the half-metallic Heusler compound Co_2HfSn: Evidence from critical behavior combined with first-principles calculations

Azizur Rahman,[1,*] Majeed Ur Rehman,[2,*] Hongze Zhao,[1] Wei Liu,[3] Jianlin Wang,[4,5] Yalin Lu,[4,5] Keqing Ruan,[1,6] Rucheng Dai,[7] Zhongping Wang,[7] Xiaoping Tao,[7] Lei Zhang,[8] and Zengming Zhang[7,6,†]

[1]*Department of Physics, University of Science and Technology of China, Hefei 230026, China*

[2]*College of Physics and Optoelectronic Engineering, Shenzhen University, Nanhai Ave 3688, Shenzhen, Guangdong 518060, China*

[3]*Institute of Physical Science and Information Technology, Anhui University, Hefei 230601, China*

[4]*Hefei National Laboratory for Physical Sciences at the Microscale, University of Science and Technology of China, Hefei 230026, China*

[5]*Anhui Laboratory of Advanced Photon Sciences and Technology, University of Science and Technology of China, Hefei 230026, China*

[6]*Key Laboratory of Strongly-Coupled Quantum Matter Physics, Chinese Academy of Sciences, School of Physical Sciences, University of Science and Technology of China, Hefei, Anhui 230026, China*

[7]*The Centre for Physical Experiments, University of Science and Technology of China, Hefei 230026, China*

[8]*High Magnetic Field Laboratory, Chinese Academy of Sciences, Hefei 230031, China*

(Received 30 November 2020; revised 6 February 2021; accepted 25 February 2021; published 17 March 2021)

Co_2-based Heusler alloys show diverse magnetic behavior, extending from the localized Heisenberg to the delocalized itinerant, and thus cannot be generalized with one specific model. Therefore, we bring together experiments and first-principles calculations to reveal the origin of long-range ferromagnetism in the Co_2-based Heusler alloy Co_2HfSn. The precise value of the critical exponents $\beta = 0.471(4)$, $\gamma = 1.02(4)$, and $\delta = 3.273(5)$ with the Curie temperature ($T_c = 430$ K) were determined experimentally by means of different analytical methods such as modified Arrott plot analysis, the Kouvel-Fisher method, and critical isotherm analysis. The deduced critical exponents belong to the theoretical prediction of the three-dimensional mean-field model. The magnetic exchange distance is found to decay as $J(r) \sim r^{-4.52}$, indicating the long-range magnetic interaction in Co_2HfSn. Moreover, the magnetic entropy change $-\Delta S_M$ features a maximum at T_c, i.e., $-\Delta S_M^{\max} \sim 29.87(6)$ J kg^{-1} K^{-1} at 5 T, whereas power law fitting of $-\Delta S_M^{\max}$ with H gives $n' = 0.663(5)$, also confirming the mean-field-type magnetic interaction in Co_2HfSn. Meanwhile, in order to explore the origin of long-range ferromagnetic ordering in Co_2HfSn, spin-polarized density functional theory calculations were employed in this study. No stable antiferromagnetic solution with stable local magnetic moments at the Co or Hf site was observed in our fixed spin moment simulation, revealing that Co_2HfSn is a highly itinerant magnet with a long-range ferromagnetic solution together with robust half-metallic conduction stable against thermal excitation higher than room temperature. Furthermore, our theoretical analysis shows that Co_2HfSn belongs to an unconventional family of itinerant magnetism. Both the 100% spin-polarized metallicity and ferromagnetism arise from the Co d orbitals, causing it to be unique compared to the conventional itinerant family of Ni, Co, or Fe, where magnetism and metallicity originate from different orbitals characters.

DOI: 10.1103/PhysRevB.103.094425

I. INTRODUCTION

Half metallicity has been the subject of significant scientific interest for the last three decades since the theoretical prediction of 100% spin polarization in the half-Heusler NiMnSb [1] and later in the full-Heusler Co_2MnSn [2]. Recent progress on this phenomenon has been applied broadly to systems, like the D_0 d half Heusler [3,4], Dirac half metals [5,6], Weyl semimetals [7,8], and even perovskites [9,10]. Their low Curie temperatures, however, inhibit their application at room temperature and limit their significance. On the other hand, the transition metal based Heusler alloy system possesses half metallicity accompanied by high Curie temperatures, negligible spin-orbit coupling, and scalability of electronic properties [11–19]. Heusler alloys, intermetallic compounds, also known as full-Heusler alloys, are crystallized in the X_2YZ stoichiometric composition, whereas half-Heusler alloys are designed in the XYZ stoichiometric composition. Heusler alloys have been known since the early 19th century. However, they have recently had a remarkable comeback due to their high spin polarization and potential applications in spintronics devices. Co_2YZ (where Y is a transition metal and Z is a main group element), an important subset of Heusler alloys, attracted significant interest due to additional properties, such as magnetic damping [20], large negative magnetoresistance [21], anomalous Hall conductivity [22], and large spin polarization and high Curie temperature T_c [23,24]. Due to such fascinating characteristics, Co_2-based Heusler alloys such as Co_2MnSi, Co_2MnGe, $Co_2FeAl_{0.5}Si_{0.5}$, and Co_2XY (X = Ti or Hf, Y = Si, Ge, or Sn) have been extensively studied for many interesting phenomena both theoretically and experimentally [11–24]. Because of the predicted large

*These authors contributed equally to this work.
†Corresponding author: zzm@ustc.edu.cn

spin gap and high T_c, Co_2-based alloys remain the focus of applications in future spintronic device technology operating above room temperature.

On the other hand, the origin of ferromagnetism in Co_2-based half-metallic Heusler alloys is not straightforward and remains one of the interesting problems in magnetism. For the magnetization these alloys obey the Slater-Pauling rule ($M_{tot} = Z'_{tot} - 24$), where M and Z' represent the magnetic moment and number of valence electrons, respectively, leading to the characteristic integer magnetic moment [25]. Their exchange interaction can be described by the Heisenberg Hamiltonian, and thus, these materials are traditionally believed to be localized magnetic moment systems [26]. However, several theoretical and experimental studies recognized the presence of complex exchange interactions of the localized magnetic moments [2,27–29] in these alloys and thus strong deviation in their spin exchange interactions from the Heisenberg model [30,31]. Very recently, a critical behavior study around the paramagnetic to ferromagnetic (PM-FM) transition in Co_2TiGe revealed spin interaction is mean-field-like [30]. Both the short-range direct exchange coupling between nearest neighbors and coupling between further neighbor spins (indirect exchange coupling) mediated by Ruderman-Kittel-Kasuya-Yosida interaction are assumed to be responsible for mean field-like long range spin interaction in Co_2TiGe. Similarly, our previous investigation realized the long-range spin interaction in Co_2TiSn, which is due to the competition between the magnetic interaction of itinerant minority spins and localized majority spins [31]. Furthermore, significant spin-orbit coupling that leads to the magnetocrystalline anisotropy in Co_2-based alloys, and thus anisotropic exchange interaction, may also play a role in magnetic ordering in these systems. Therefore, this class of materials, i.e., Co_2-based Heusler alloys, yields versatile ferromagnetic half metals. This family of compounds needs to be explored further for its detailed magnetic properties. Understanding the magnetic mechanism in these systems is key to practical use of these materials in device applications. Analysis of the critical exponents associated with the PM-FM transition is an effective method for the identification of the magnetic mechanism and properties.

In this work, we combine experiments with theoretical calculations to study the detailed magnetic properties of a high-T_c half-metallic ferromagnet, Co_2HfSn. The nature of the exchange interaction is experimentally investigated by a critical behavior study in the vicinity of the PM-FM transition in Co_2HfSn, which is found to be consistent with the theoretical prediction of the three-dimensional (3D) mean field. However, the spin-polarized density functional theory (DFT) calculations revealed that Co d highly itinerant electrons are responsible for both long-range ferromagnetism and conductivity in this material system.

II. METHODS

A. Experimental and calculation details

An ordered Heusler alloy Co_2HfSn was synthesized via repeated melting of the stoichiometric composed mixtures of 99.9% pure Hf, 99.9% pure Co, and 99.999% pure Sn in an argon arc furnace. The reaction product was then sealed in a quartz tube together with an appropriate quantity of argon gas and heated at 860 °C for 2 weeks and then quenched in water to achieve a homogenized sample. The structure and phase purity of Co_2HfSn were characterized by x-ray diffraction (XRD; Rigaku SmartLab) with Cu K_α radiation. The magnetization of the samples was measured by a superconducting quantum interference device vibrating-sample magnetometer (Quantum Design). The sample was processed to form an ellipsoid and to reduce the demagnetizing field; the magnetic field was applied along the longest semiaxis. For the magnetization measurement the procedure used in Ref. [32] was adopted. For theoretical calculations, the first-principles spin-polarized strategy was used under the projector augmented wave method [33], as implemented in the Vienna Ab initio Simulation Package (VASP) [34]. To address the exchange-correlation functional, the Perdew-Burke-Ernzerhof scheme was used with the cutoff energy for the basis function to be 550 eV. The Brillouin zone was sampled using a $20 \times 20 \times 20$ Monkhorst-Pack [35] k-point mesh.

B. Scaling hypothesis

The second-order phase transition around T_c shows the critical behavior of the various thermodynamic variables, which are governed by critical fluctuations. The critical behavior is characterized by the set of interrelated statistical critical exponents α, γ, δ, η, and ν. The exponent α can be obtained from specific heat, from spontaneous magnetization below T_c; γ can be obtained from inverse magnetic susceptibility above T_c, and δ can be obtained from the magnetization isotherm at T_c. From magnetization measurements, these exponents are mathematically described as follows [36,37]:

$$M_s(T) = M_0(-\varepsilon)^\beta, \quad \varepsilon < 0, \tag{1}$$

$$\chi_0^{-1}(T) = (h_0/M_0)(\varepsilon)^\gamma, \quad \varepsilon > 0, \tag{2}$$

$$M = DH^{1/\delta}, \quad \varepsilon = 0, \quad T = T_c, \tag{3}$$

where $\epsilon = (T - T_c)/T_c$ is the reduced temperature and h_0/M_0 and D are critical amplitudes. The magnetic equation of state in the asymptotic critical region can be written as follows [37]:

$$M(H, \varepsilon) = \varepsilon^\beta f_\pm\left(H/\varepsilon^{\beta+\gamma}\right), \tag{4}$$

where f_+ ($T > T_c$) and f_- ($T < T_c$) are the regular functions. Equation (4) can be further expressed in terms of renormalized magnetization $m \equiv M(H, \epsilon)\epsilon^{-\beta}$ and renormalized field $h \equiv \epsilon^{-(\beta+\gamma)}$ as

$$m = f_\pm h. \tag{5}$$

Equation (5) suggests that for a true scaling relation and the right choice of critical exponents α, β, and γ renormalized m and h will form two independent branches above and below T_c, respectively.

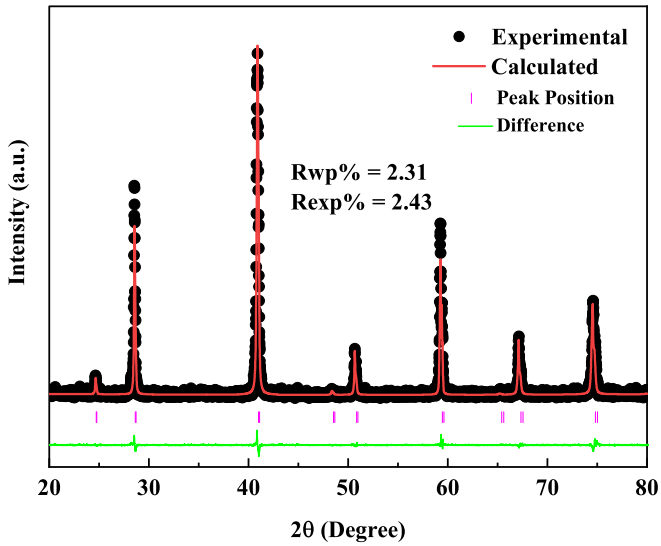

FIG. 1. (a) Refined powder XRD pattern of Co_2HfSn at room temperature. The solid black spheres represent the experimental data, and the solid red line shows the calculated result. The vertical purple lines show the Bragg positions, and the solid green line at the bottom corresponds to the difference between the experimental and fitted intensities.

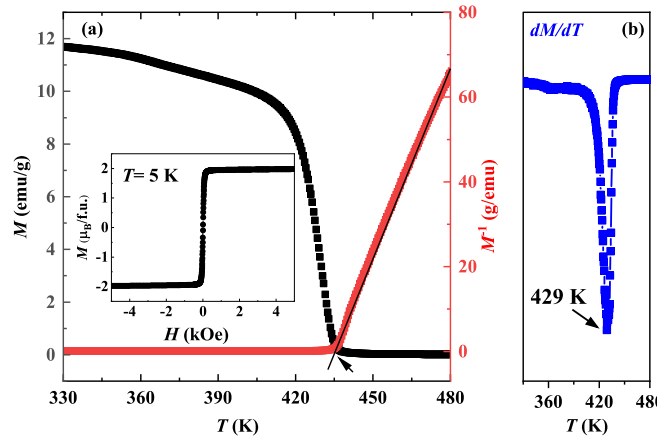

FIG. 2. (a) Temperature dependence of magnetization $M(T)$ on the left and $M^{-1}(T)$ on the right. The inset shows the field dependence of magnetization measured at 5 K. (b) The derivative magnetization dM/dT vs T.

III. RESULTS AND DISCUSSION

Figure 1 shows the powder XRD measurement Co_2HfSn sample at room temperature. The XRD data are refined for phase purity and structural parameters using materials analysis using diffraction. The XRD refinement details can be found elsewhere. The obtained fitting parameters $R_{wp} = 2.31\%$ and $R_{\text{exp}} = 2.43\%$ with goodness of fit approaching 1 suggest that the Co_2HfSn Heusler alloy shows an almost perfect degree of order as the $L2_1$ phase within the XRD resolution limits. It is very important to recognize such an order phase in Co_2HfSn since $A2$ type, $B2$ type, or $D0_3$ type usually inhibits spin polarization of Heusler alloys [38]. The lattice parameter was determined to be $a = 6.23(6)$Å, in agreement with earlier reported values [25,39].

Figure 2(a) presents the magnetization vs temperature curve $M(T)$ and inverse magnetization $M^{-1}(T)$ of Co_2HfSn at a magnetic field of 100 Oe. The PM-FM transition is observed at around 429 K, estimated by the temperature derivative of the magnetization as shown in Fig. 2(b). The $M^{-1}(T)$ curve shows a deviation from the straight line above T_c, indicating that critical fluctuations occur even in the PM region. As we already mentioned, the half-metallic Heusler alloys obey the Slater-Pauling, $M = (Z' - 24)$, rule for magnetization, where M is the total magnetization and Z' is the number of total valence electrons. In this context, Co_2HfSn should display a magnetic moment of $2\mu_B$, as Z' is 26 for Co_2HfSn. Thus, the magnetic field dependence of the dc magnetization is measured at 2 K and shown in the inset of Fig. 2(a). The saturation magnetization is estimated to be $1.993\mu_B$/f.u., indicating the compound obeys the Slater-Pauling rule. To characterize PM-FM transition in Co_2HfSn, a series of magnetization isotherms is measured by an interval of $\Delta T = 1$ K around the estimated T_c (determined from the dM/dT curve), as shown in Fig. 3(a).

The conventional Arrott plot is constructed by plotting M^2 vs H/M to check whether the Landau mean-field theory of the magnetic phase transition holds for Co_2HfSn. In the case of the mean-field values of the critical exponents ($\beta = 0.5$ and $\gamma = 1$), the Arrott plot must produce a series of parallel straight lines; the one that passes through the origin corresponds to the magnetic isotherm at T_c. Figure 3(b) displays the Arrott plot for Co_2HfSn around T_c. All the lines are quasistraight lines with a downward curvature, suggesting that the nature of the magnetic exchange mechanism is mean-field-like. However, the lines are not very straight, and there is no line passing through the origin, which implies that critical exponents need to be modified under the framework of the Landau mean-field model in order for us to obtain a precise value of T_c. Furthermore, the downward curvature of these lines shows that the nature of the PM-FM phase transition is second order [40].

In order to determine the true values of the critical exponents as well as T_c, the magnetization is reanalyzed using the modified Arrott plot analysis [41] based on the following equation:

$$(H/M)^{1/\gamma} = A(T - T_c/T) + BM^{1/\beta}, \tag{6}$$

where A and B are considered to be constants. A rigorous iterative method is used to prevent nonphysical fitting and systematic errors in exponent values. The initial values of $M_s(T)$ and $\chi_0^{-1}(T)$ are taken from the Arrott plot shown in Fig. 3(b) by linear extrapolation of the isotherms from the high field to the intercepts with the $M^{1/\beta}$ and $(H/M)^{1/\gamma}$ axes, respectively. A new set of β and γ can be determined using Eqs. (1) and (2). These new values of β and γ are used to construct a new Arrott plot similar to that in Fig. 3(b). The process is repeated until stable values of β, γ, and T_c are achieved. Using this approach, the critical exponents obtained are hardly dependent on the initial parameters, showing that these critical exponents are intrinsic and reliable. The final modified Arrott plot constructed with the critical exponent values, $\beta = 0.471$ and $\gamma = 1.02$, is displayed in Fig. 4. It is evident from Fig. 4 that all the lines are very straight to each

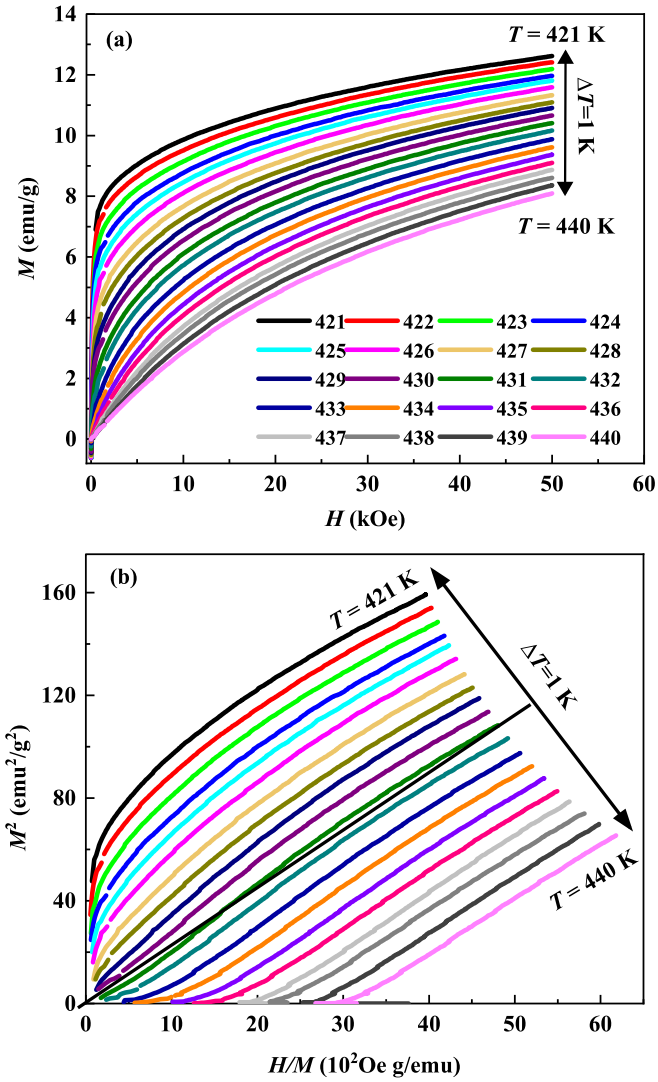

FIG. 3. (a) The initial isothermal magnetization curves around T_c. (b) Arrott plot of H/M vs M^2 around T_c.

other in the high-field region and the line at $T_c = 430$ K passes through the origin.

Figure 5(a) is generated by plotting the finally obtained $M_s(T)$ and $\chi_0^{-1}(T)$ values as a function of temperature. Using these values of $M_s(T)$ and $\chi_0^{-1}(T)$, fitting Eqs. (1) and (2) yields $\beta = 0.469(6)$, $\gamma = 1.0412(5)$, $T_c = 429.823(4)$ and $\beta = 0.473(6)$, $\gamma = 1.0322(4)$, $T_c = 431.263(5)$, respectively. The values of the critical exponents and T_c obtained here are consistent with those obtained using the modified Arrott plot analysis.

Alternatively, to obtain precise values of β, γ, and T_c, we us the Kouvel-Fisher (KF) method [42] using Eqs. (7) and (8),

$$\frac{M_s(T)}{dM_S(T)/dT} = \frac{T - Tc}{\beta}, \tag{7}$$

$$\frac{\chi_0^{-1}(T)}{d\chi_0^{-1}(T)/dT} = \frac{T - Tc}{\gamma}. \tag{8}$$

By this method, the straight-line fitting of $M_s(dM_s/dT)$ vs T and $\chi_0^{-1}(d\chi_0^{-1}/dT)$ yields slopes of $1/\beta$ and $1/\gamma$, respectively. The best part of this method is that no prior

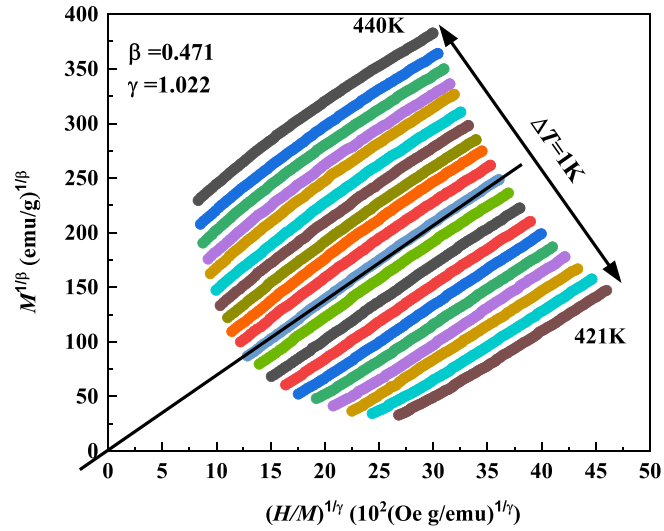

FIG. 4. The modified Arrott plot around T_c for the optimum fitting with $\beta = 0.471$ and $\gamma = 1.02$.

information is needed about the critical temperature. Using the KF method as shown in Fig. 5(b), the new obtained values are $\beta = 0.465(4)$ and $\gamma = 1.0614(5)$, with $T_c = 429.723(4)$, and $\beta = 0.477(4)$ and $\gamma = 1.0296(5)$, with $T_c = 431.622(4)$. It is worth noting that the values of critical exponents as well as T_c obtained using the KF method and modified Arrott plot analysis are fairly well matched. This implies that the obtained values are unambiguous and self-consistent.

The reliability of derived critical exponents and T_c using a variety of methods can be tested by scaling analysis. Based on Eq. (5), the renormalized m is plotted vs the renormalized h in Fig. 5(c). The inset in Fig. 5(c) shows the same plot on a log-log scale. It is very remarkable that all data collapse into two different branches for $T > T_c$ and $T < T_c$. Alternatively, the reliability of critical exponents and T_c is further confirmed with a more rigorous method by plotting m^2 vs h/m. Figure 5(d) shows such a plot, where it is observed that all the data collapse into two universal curves: one for $T > T_c$ and another for $T < T_c$. This clearly demonstrates that interactions are renormalized properly in the critical regime following a scaling state equation.

Using the above critical exponents, the critical temperature is determined to be 430 K. Figure 6 shows the magnetic isotherm measured at 430 K. The inset in Fig. 6 shows the log-log scale plot of the same measurement. Following Eq. (3), the log-log scale fitting yields a straight line with a slope of $1/\delta$. This gives the value of the third critical exponent, $\delta = 3.273(5)$. Alternatively, δ can be determined by the Widom scaling relation [43] as follows:

$$\delta = 1 + \frac{\gamma}{\beta}. \tag{9}$$

Following Eq. (9), using the values deduced by the KF method and modified Arrott plot analysis, the values of $\delta = 3.165(5)$ and $\delta = 3.282(4)$, respectively, are matched reasonably well with the values obtained from critical isotherm analysis. The values obtained for the critical exponents using different analytical methods are summarized in Table I along with those

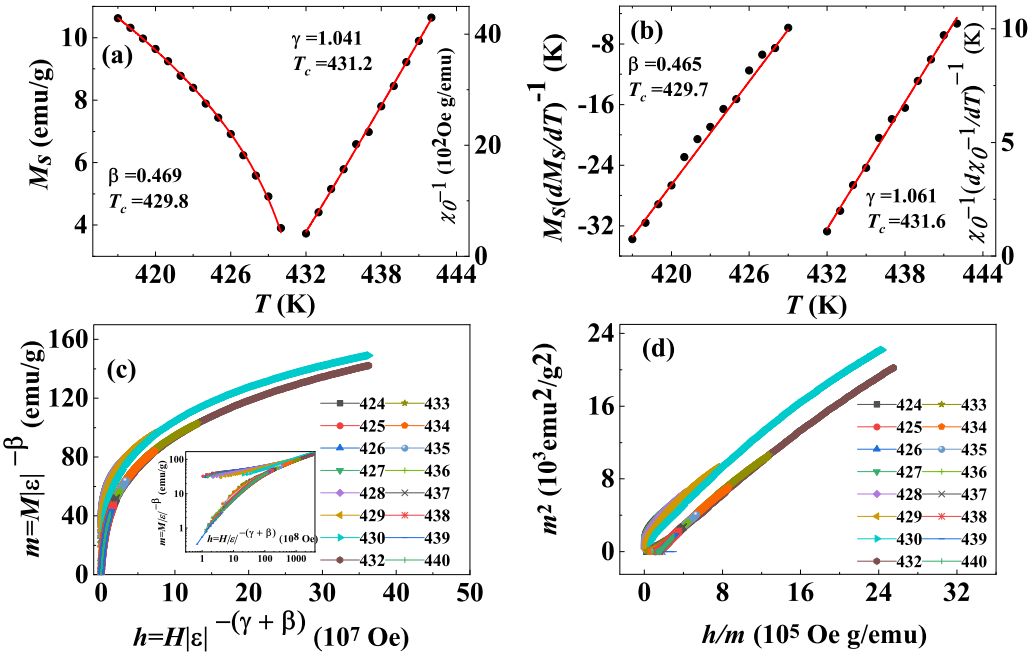

FIG. 5. (a) The spontaneous magnetization M_s (left) and inverse initial susceptibility χ_0^{-1} (right) vs T with the fitting solid curves. (b) KF plots for $M_s(T)$ (left) and $\chi_0^{-1}(T)$ (right; solid lines are fitted). (c) Scaling plots around T_c using β and γ determined by the KF method. (d) The renormalized magnetization and field potted as m^2 vs h/m.

from different theoretical models. It has been found that critical exponents derived in this work are similar to that of the mean-field model, indicating long-range magnetic ordering in Co_2HfSn.

The universality class of the magnetic phase transition in a homogeneous magnet depends on the exchange distance $J(r)$. Fisher *et al.* [48] treated such magnetic ordering as an attractive spin-spin interaction, where the renormalization group theory analysis showed that the long-range interactions decay with distance r as follows:

$$J(r) \sim 1/r^{(d+\sigma)}, \tag{10}$$

where d is the spatial dimensionality and σ is a positive constant. According to this model, the spin interaction is long range or short range depending on $\sigma > 2$ or $\sigma < 2$. Moreover, it predicts the susceptibility exponent γ, which has been determined by the renormalization group approach as follows:

$$\gamma = 1 + \frac{4}{d}\left(\frac{n+2}{n+8}\right)\Delta\sigma + \frac{8(n+2)(n-4)}{d^2(n+8)^2} \times \left[1 + \frac{2G\left(\frac{d}{2}\right)(7n+20)}{(n-4)(n+8)}\right]\Delta\sigma^2, \tag{11}$$

where $\Delta\sigma = (\sigma - \frac{d}{2})$, $G(\frac{d}{2}) = 3 - \frac{1}{4}(\frac{d}{2})^2$, and n represents the spin dimensionality. In the case of 3D materials with isotropic spins, $J(r) \sim 1/r^{(3+\sigma)}$, with $3/2 \leqslant \sigma \leqslant 2$. The Heisenberg model is valid for an isotropic 3D ferromagnet when $\sigma = 2$, where $J(r)$ decays faster than r^{-5}. For $\sigma = 3/2$, the mean-field model is realized, showing that $J(r)$ drops slower than $r^{-4.5}$. In the current work, σ is determined to be 1.516(3); then the correlation length critical exponent $\nu = 0.572(8)$, and $\alpha = 0.020(1)$. It has been realized that the magnetic exchange mechanism $J(r)$ decays as $r^{-4.52}$, suggesting mean-field-like, long-range spin interaction in Co_2HfSn.

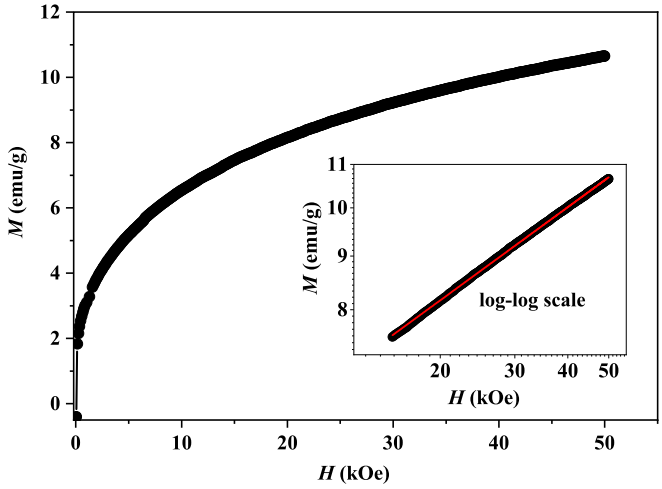

FIG. 6. Field dependence of the magnetization isotherm at $T_c =$ 430 K for Co_2HfSn. The inset shows the same plot in $\log_{10}$-$\log_{10}$ scale, where the solid line is the linear fit following Eq. (3) that gives the critical exponent δ.

Next, we would like to estimate the magnetic entropy change in Co_2HfSn, as it can explore materials' magnetocaloric characteristics as well as intrinsic magnetic interaction. Magnetic entropy change can be calculated using Maxwell's relation $[\partial S(T,H)/\partial H]_T = [\partial M(T,H)/\partial T]_H$,

TABLE I. Comparison of critical exponents of Co_2HfSn with different theoretical models. MAP, modified Arrott plot; KF, Kouvel-Fisher method; CI, critical isotherm analysis.

Composition	References	Technique	β	γ	δ
Co_2HfSn	This work	MAP	0.472(3)	1.021(2)	3.16(2)
	This work	KF	0.477(4)	1.0296(5)	3.15(7)
	This work	CI			3.273(5)
Mean field	[37]	Theory	0.5	1.0	3.0
3D Heisenberg	[40,44]	Theory	0.365	1.386	4.8
3D XY	[40,45]	Theory	0.345	1.316	4.81
3D Ising	[40,45]	Theory	0.325	1.24	4.82
Ni	[46]	KF	0.391(10)	1.314(16)	4.39(2)
Co_2TiGe	[30]	KF	0.495(2)	1.324(4)	3.675
Co_2TiSn	[31]	KF	0.537(2)	1.255(3)	3.33(7)
$Gd_{80}Au_{20}$	[47]	KF	0.44(2)	1.29(5)	3.96(3)

which can also be written as follows:

$$\Delta S_M(T,H) = S_M(T,H) - S_M(T,0) = \int_0^{H^{\max}} \left[\frac{\partial M(T,H)}{\partial T}\right]_H dH. \quad (12)$$

In the case of magnetic isotherms measured at a discreet small magnetic field, as shown in Fig. 3(a), $\Delta S_M(T,H)$ can be estimated as [49]

$$\Delta S_M(T_i,H) = \frac{\int_0^H M(T_i,H)dH - \int_0^H M(T_{i+1},H)dH}{T_i - T_{i+1}}. \quad (13)$$

Figure 7(a) shows the plot of $-\Delta S_M$ versus temperature at different applied magnetic fields. Each curve shows a peak at T_c, indicating the magnetic entropy change reaches its maximum at T_c for any field. The highest value of $-\Delta S_M$ is estimated to be 28.2 J kg^{-1} K^{-1}. This sufficiently large value of magnetic entropy change indicates that Co_2HfSn can be used as a high-temperature magnetic refrigerant material.

Scaling analysis can be constructed by normalizing all the $-\Delta S_M$ curves against the corresponding $-\Delta S_M^{\max}$, whereas temperature is normalized into rescaled temperature θ, defined in the following equation [50]:

$$\theta = \begin{cases} \theta_- = (T_c - T)/(T_{r1} - T_c), & T \leqslant T_c, \\ \theta_+ = (T - T_c)/(T_{r2} - T_c), & T > T_c, \end{cases} \quad (14)$$

where T_{r1} and T_{r2} are the reference temperatures above and below T_c, respectively. Here T_{r1} and T_{r2} correspond to $\Delta S_M(T_{r1},T_{r2}) = \frac{1}{2}\Delta S_M^{\max}$. Using this method, all the $-\Delta S_M(T,H)$ curves collapsed into a single universal curve in the vicinity of T_c, independent of the applied magnetic field, as shown in Fig. 7(b). Convergence of $-\Delta S_M(T,H)$ describes the type of magnetic transition (PM-FM) in Co_2HfSn is second order. In the framework of the mean-field model, $-\Delta S_M^{\max} = -1.07qR(g\mu_B JH/k_B T_c)^{2/3} \propto H^{2/3}$, where q, R, and g represent total magnetic ions, the gas constant, and the Landé factor, respectively [51]. More universally, $-\Delta S_M^{\max}$ follows a power law dependence on the magnetic field, i.e., $-\Delta S_M^{\max} = aH^{n'}$, where n' is dependent on the magnetic state of the sample. The power law fitting of $-\Delta S_M^{\max}$ with H yields $n' = 0.663(5)$, as shown in Fig. 7(b). The value of n' is very close to the typical value of 2/3 for the mean-field model, indicating the magnetic entropy change in the vicinity

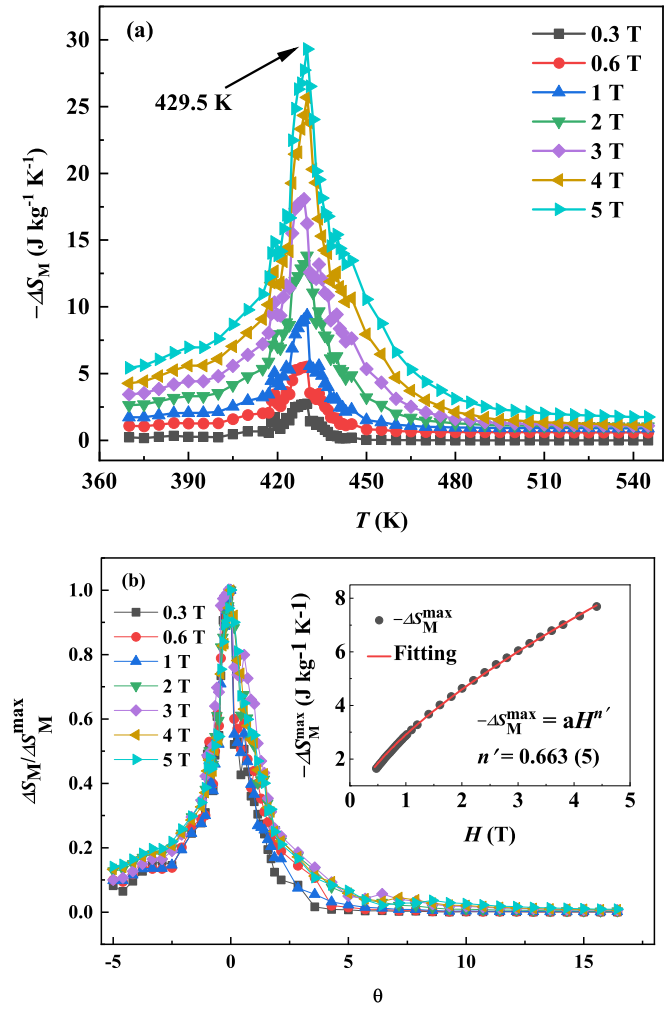

FIG. 7. (a) The magnetic entropy change $-\Delta S_M$ obtained from magnetization at various magnetic fields. (b) Normalized $-\Delta S_M$ as a function of the rescaled temperature θ. The inset shows the magnetic field dependence of the maximum magnetic entropy change $-\Delta S_M^{\max}$ with power law fitting given by the solid red line.

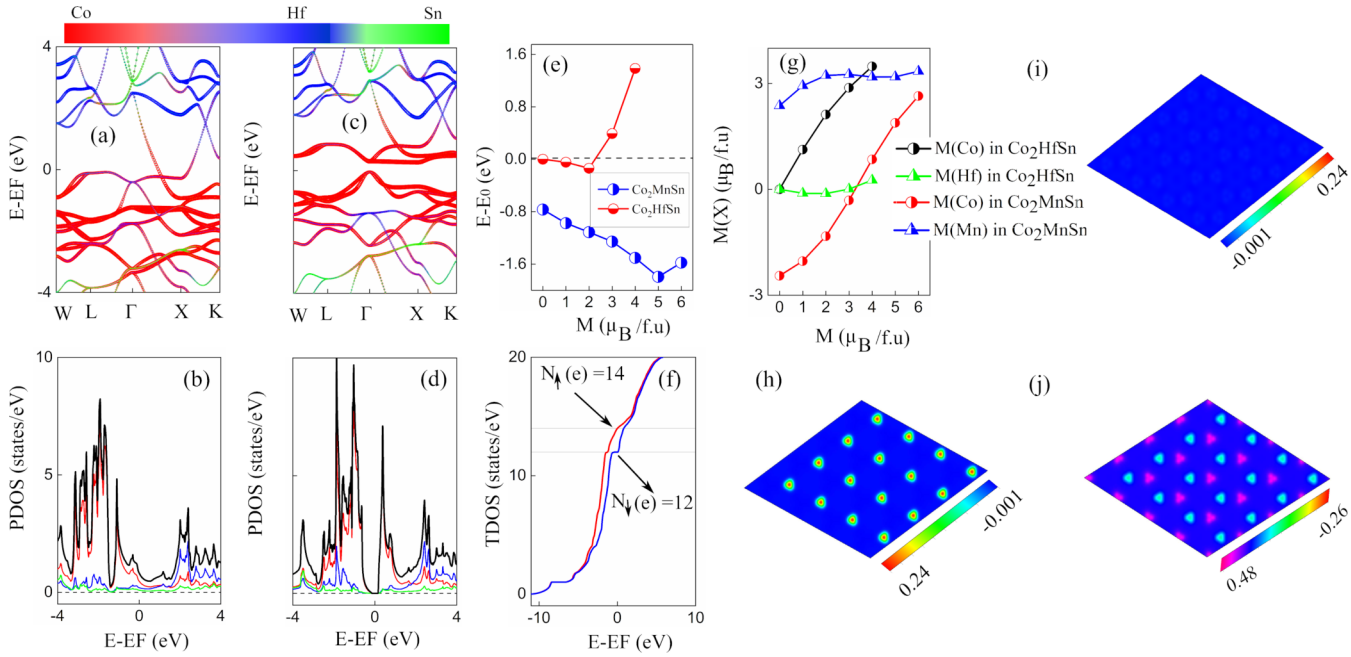

FIG. 8. These plots demonstrate our theoretical insights: Atomic resolved spin-polarized band structure for the (a) majority- and (c) minority-spin components. Atomic resolved and total spin-polarized density of states (DOS) in the (b) majority and (d) minority components. (e) The calculated energy difference between the spin-polarized and non-spin-polarized solutions under the constraint of fixing the total spin magnetic moment ranging from $0\mu_B$ to $6\mu_B$. The non-spin-polarized solution with vanishing local magnetic moments of Co under the constraint $M = 0\mu_B$ can be noted for Co_2HfSn. In comparison, the Co_2MnSn system is shown, for which the spin polarization under the constraint of $M = 0\ \mu_B$ exists. (f) The integrated DOS for Co_2HfSn where the system's magnetic moment can be understood from the difference of up- and down-spin electrons. (g) The spin moments' variations under the constraint of total magnetization ranging from $0\mu_B$ to $6\mu_B$ are shown for two Co atoms (in Co_2HfSn and Co_2MnSn) and Hf in Co_2HfSn. Distribution of spin-charge density for the Co_2HfSn system under the fixed total magnetic moment (h) $M = 2\mu_B$ and (i) $M = 0\mu_B$. The vanishing of the local spin density can be noticed in the $M = 0\mu_B$ solution. (j) For comparison, the spin-charge density under the constraint of zero total magnetic moments $M = 0\mu_B$ is also shown for the Co_2MnSn system.

of T_c also confirms the mean-field-type magnetic exchange interaction in Co_2HfSn.

To explain the long-range magnetic nature in our proposed system, Co_2HfSn, and to further assist our experimental insights through a theoretical approach, we use the DFT framework. The nature of magnetic solids depends on to what extent their magnetic moments are itinerant or localized. In the local magnetic moments limit, stable magnetic moments reside on each magnetic component, and intra-atomic interactions are responsible. The magnetism in solids is then established via these intermoment interactions, characterized by the Heisenberg or similar spin models. In the high itinerant limit, there is no survival of stable magnetic moments on the magnetic site; instead, long-range magnetism is established via conduction carriers in the system.

The atomic resolved electronic band structures and density of states (DOS), as shown in Fig. 8, demonstrating that Co_2HfSn is a type-I half-metallic solid with a majority-spin channel cross the Fermi surface, and the minority-spin channel shows semiconductor behavior. A closer inspection of the orbital projected band structures and DOS reveals that the Co d state mainly dominates around the Fermi surface [see Figs. 8(a)–8(d)]. The strength of the DOS for minority-spin carriers is higher than that of the majority-spin carriers, which is also consistent with the band structure, as it can be recognized that the minority-spin bands have relatively flat dispersion compared with majority-spin bands. The observed spin-flip band gap, defined as the ECB↓-EF, which is an important parameter indicating the stability of the half metallicity against thermal excitation, is around 270 meV higher than room temperature. As can be perceived from the integrated density of states [Fig. 8(f)] and fixed spin magnetic moment calculations [see Figs. 8(e) and 8(f)], the spin magnetic moment is about $2\mu_B$/f.u., which is entirely consistent with our experiment findings.

To elaborate on the itinerancy origin of the long-range ferromagnetic ordering in Co_2HfSn, we first validate that the magnetic moments that arise at the Co site are indeed stable. Does it originate as a result of intra-atomic interaction, or is it due to conduction electrons? For this, we carry out a series of simulations to stabilize the antiferromagnetic solution with opposite spin orientation on the Co site. Additionally, we performed the fixed moment calculation under zero net magnetization constraint. The simulations reveal that spin magnetic moments for the Co site vanish in the antiferromagnetic (AFM) arrangement with no spin polarization solution at all [see Figs. 8(e) and 8(i)]. Spin-charge densities arising from the majority $\rho_\uparrow$ and minority $\rho_\downarrow$ valence electrons are shown in Figs. 8(h)–8(j). The spin-charge density is dominantly noticeable around the Co sites in Co_2HfSn for a ferromagnetic solution [see Fig. 8(h)]. However, as can be seen from the spin-charge density under the imposed zero total moment

constraint [see Fig. 8(i)], there is no spin polarization solution exit for the Co_2HfSn system. This excludes the possibility of stable local magnetic moments and confirms the itinerary picture of the magnetism in Co_2HfSn. This theoretical findings is also consistent with our experimental insights showing long-range FM ordering in the Co_2HfSn system.

Furthermore, a shift in the majority-spin states of Co can be observed with respect to the high DOS in the minority-spin channel around the Fermi level [see Figs. 8(b) and 8(d)]. This shift appears due to itinerant bands of Co in the majority-spin states crossing the Fermi surface. For comparison and to further support our analysis, we replace the Hf atoms with Mn and use the fixed moment simulation to stabilize the AFM solution of Co_2MnSn. The spin density plot [Fig. 8(j)] and the fixed zero magnetic moment [see Fig. 8(e)] show that the spin polarization solution exists for the Co_2MnSn system with opposite moments arising from Mn and Co under the zero total magnetic moment constrained. We further simulated the system to observe the variations in the spin-state configuration of the Co ions using the fixed spin moment approach. As can be noticed from Fig. 8(g), the Co moments show considerable variations in the fixed moment calculation, whereas the Mn moments seem much stiffer against the imposing magnetization M, indicating the local (itinerant) nature of Mn (Co) in Co_2MnSn. This shows that Co_2MnSn exhibits a local moment behavior regarding the Mn while retaining the Co magnetism itinerancy. On the other hand, Co_2HfSn can be described as an utterly itinerant system with no stable local magnetic moments and spin polarization solution in the zero magnetization constraint.

It is worth mentioning that Co_2HfSn exhibits exceptional itinerant behavior with both metallicity and long-range ferromagnetism originating from the d electrons of the Co ions, which is distinct from the conventional mode as observed previously in Fe, Co, and Ni ferromagnets where the metallization and ferromagnetism mainly originate from different orbitals characters [52]. This difference is interesting and might be efficient to control the magnetism via electron conduction in Co_2HfSn and similar systems. Moreover, due to the Hf component in Co_2HfSn, the spin-orbit coupling and magnetic anisotropy might be strong, and two-dimensional ferromagnetism can thus be stabilized by epitaxially growing Co_2HfSn in a thin-film geometry.

IV. CONCLUSION

In summary, we combined experiments with theoretical calculations to present a comprehensive analysis of the magnetic properties of the half-metallic Heusler alloy Co_2HfSn. Co_2HfSn was synthesized in the $L2_1$ chemical structure with $a = 6.23(6)$ and in the $Fm\bar{3}m$ space group. The critical behavior study around T_c identified the PM-FM phase transition as second order in nature. The critical exponents β, γ, and δ obtained via different experimental techniques match well with the theoretical prediction of the 3D mean-field model. It was found that spin interaction decays as $J(r) \sim r^{-4.52}$, indicating long-range ferromagnetic ordering in Co_2HfSn. Spin-polarized DFT calculations were carried out in order to provide deep insight into the long-range ferromagnetic order in Co_2HfSn. This study suggests that highly itinerant electrons stabilize the long-range ferromagnetic interaction with a remarkably high T_c in Co_2HfSn. Furthermore, it was also revealed that both the half-metallic conductivity and ferromagnetism emerge from the Co d electrons, making Co_2HfSn unique in that both the conductivity and magnetism can be tuned from a single origin.

ACKNOWLEDGMENTS

This work was supported by the National Natural Science Foundation of China (Grants No. 12074360, No. 21905263, and No. 12004366) and the Science Challenge Project (Grant No. TZ2016001).

[1] R. A. de Groot, F. M. Mueller, P. G. van Engen, and K. H. J. Buschow, Phys. Rev. Lett. **50**, 2024 (1983).
[2] J. Kübler, A. R. William, and C. B. Sommers, Phys. Rev. B **28**, 1745 (1983).
[3] S. Davatolhagh and A. Dehghan, Phys. C (Amsterdam, Neth.) **552**, 53 (2018).
[4] A. Dehghan and S. Davatolhagh, J. Alloys Compd. **772**, 132 (2019).
[5] Q. Sun and N. Kioussis, Phys. Rev. B **97**, 094408 (2018).
[6] F. Ma, Y. Jiao, Z. Jiang, and A. Du, ACS Appl. Mater. Interfaces **10**, 36088 (2018).
[7] Q. Xu, E. Liu, W. Shi, L. Muechler, J. Gayles, C. Felser, and Y. Sun, Phys. Rev. B **97**, 235416 (2018).
[8] Q. Wang, Y. Xu, R. Lou, Z. Liu, M. Li, Y. Huang, D. Shen, H. Weng, S. Wang, and H. Lei, Nat. Commun **9**, 3681 (2018).
[9] H. Hsu and S.-C. Huang, Phys. Rev. Mater. **2**, 111401(R) (2018).
[10] N. Kim, R. Kim, and J. Yu, J. Magn. Magn. Mater **460**, 54 (2018).
[11] S. Ishida, S. Fujii, S. Kashiwagi, and S. Asano, J. Phys. Soc. Jpn. **64**, 2152 (1995).
[12] K. Inomata, S. Okamura, R. Goto, and N. Tezuka, Jpn. J. Appl. Phys. **42**, L419 (2003).
[13] T. Kubota, Z. Wen, and K. Takanashi, J. Magn. Magn. Mater **492**, 165667 (2019).
[14] K. Kodama, T. Furubayashi, H. Sukegawa, T. M. Nakatani, K. Inomata, and K. Hono, J. Appl. Phys. **105**, 07E905 (2009).
[15] T. Graf, C. Felser, and S. S. Parkin, Prog. Solid. State Chem. **39**, 1 (2011).
[16] B. Pradines, R. Arras, I. Abdallah, N. Biziere, and L. Calmels, Phys. Rev. B **95**, 094425 (2017).
[17] X. Wang, Z. Cheng, Y. Jin, Y. Wu, X. Dai, and G. Liu, J. Alloys Compd. **734**, 329 (2018).
[18] J.-X. Wang, Z. Chen, and Y. Gao, J Phys. Chem. Solids **116**, 72 (2018).
[19] L. Siakeng, G. M. Mikhailov, and D. P. Rai, J. Mater. Chem. C **6**, 10341 (2018).

[20] S. Husain, S. Akansel, A. Kumar, P. Svedlindh, and S. Chaudhary, Sci. Rep **6**, 28692 (2016).
[21] T. Block, C. Felser, G. Jakob, J. Ensling, B. Mühling, P. Gütlich, and R. Cava, J. Solid State Chem. **176**, 646 (2003).
[22] A. Husmann and L. J. Singh, Phys. Rev. B **73**, 172417 (2006).
[23] S. Wurmehl, G. H. Fecher, H. C. Kandpal, V. Ksenofontov, C. Felser, and H.-J. Lin, Appl. Phys. Lett. **88**, 032503 (2006).
[24] J. Kübler, G. H. Fecher, and C. Felser, Phys. Rev. B **76**, 024414 (2007).
[25] S. Babiker A., G. Gao, and K. Yao, J. Magn. Magn. Mater **441**, 356 (2017).
[26] N. D. Telling, P. S. Keatley, G. van der Laan, R. J. Hicken, E. Arenholz, Y. Sakuraba, M. Oogane, Y. Ando, K. Takanashi, A. Sakuma, and T. Miyazaki, Phys. Rev. B **78**, 184438 (2008).
[27] J. Thoene, S. Chadov, G. Fecher, C. Felser, and J. Kübler, J. Phys. D **42**, 084013 (2009).
[28] Y. Kurtulus, R. Dronskowski, G. D. Samolyuk, and V. P. Antropov, Phys. Rev. B **71**, 014425 (2005).
[29] E. Şaşıoğlu, L. M. Sandratskii, P. Bruno, and I. Galanakis, Phys. Rev. B **72**, 184415 (2005).
[30] S. Roy, N. Khan, R. Singha, A. Pariari, and P. Mandal, Phys. Rev. B **99**, 214414 (2019).
[31] A. Rahman, M. ur Rehman, D. Zhang, M. Zhang, X. Wang, R. Dai, Z. Wang, X. Tao, L. Zhang, and Z. Zhang, Phys. Rev. B **100**, 214419 (2019).
[32] A. K. Pramanik and A. Banerjee, Phys. Rev. B **79**, 214426 (2009).
[33] P. E. Blöchl, Phys. Rev. B **50**, 17953 (1994).
[34] G. Kresse and J. Furthmüller, Phys. Rev. B **54**, 11169 (1996).
[35] H. J. Monkhorst and J. D. Pack, Phys. Rev. B **13**, 5188 (1976).
[36] M. E. Fisher, Rep. Prog. Phys. **31**, 418 (1968).
[37] H. E. Stanley, *Phase Transitions and Critical Phenomena* (Clarendon, Oxford, 1971).
[38] Y. Miura, K. Nagao, and M. Shirai, Phys. Rev. B **69**, 144413 (2004).
[39] A. Aguayo and G. Murrieta, J. Magn. Magn. Mater **323**, 3013 (2011).
[40] B. Banerjee, Phys. Lett. **12**, 16 (1964).
[41] A. Arrott and J. E. Noakes, Phys. Rev. Lett. **19**, 786 (1967).
[42] L. P. Kadanoff, Phys. Phys. Fiz. **2**, 263 (1966).
[43] B. Widom, J. Chem. Phys. **43**, 3892 (1965).
[44] M. Campostrini, M. Hasenbusch, A. Pelissetto, P. Rossi, and E. Vicari, Phys. Rev. B **65**, 144520 (2002).
[45] J. C. Le Guillou and J. Zinn-Justin, Phys. Rev. B **21**, 3976 (1980).
[46] M. Seeger, S. N. Kaul, H. Kronmüller, and R. Reisser, Phys. Rev. B **51**, 12585 (1995).
[47] S. J. Poon and J. Durand, Phys. Rev. B **16**, 316 (1977).
[48] M. E. Fisher, S.-k. Ma, and B. G. Nickel, Phys. Rev. Lett. **29**, 917 (1972).
[49] J. Amaral, M. Reis, V. Amaral, T. Mendonça, J. Araújo, M. Sá, P. Tavares, and J. Vieira, J. Magn. Magn. Mater **290–291**, 686 (2005).
[50] V. Franco and A. Conde, Int. J. Refrig. **33**, 465 (2010).
[51] H. Oesterreicher and F. T. Parker, J. Appl. Phys. **55**, 4334 (1984).
[52] H. Capellmann, Z. Phys. B **34**, 29 (1979).